NUMERICAL STUDIES OF UNREACTIVE CONTRACTILE NETWORKS

M. DEMBO, M. MALTRUD, AND F. HARLOW
Theoretical Division, Group T-10, Mail Stop K710, Los Alamos National Laboratory, Los Alamos, New Mexico 87545

ABSTRACT We present a finite difference algorithm for integrating the reactive flow model of contractile biological polymer networks on a fixed Eulerian mesh. We discuss the accuracy and limits of the algorithm. To illustrate the application of the algorithm, we carry out a family of computations involving an unreactive contractile network contained in a two-dimensional square reaction vessel. By numerical experiments using different values of the physical parameters of the model, we find that for this simple sort of system two major dynamical modes of contraction are predicted to occur. There is the squeezing type contraction in which the network contracts to a single small clump with gradual expulsion of solution material, and the rending type contraction in which the network tears itself into a number of separate pieces. We find that to a good approximation the transition between the squeezing mode and the rending mode is controlled by a single nondimensional number (the rending number). We discuss the relevance of these results for the analysis of various experimental observations.

INTRODUCTION

The reactive flow model is a model of motile cytoplasm based on the notion of interpenetrating reactive flow (Dembo and Harlow, 1985). In the reactive flow model the cytoplasm is viewed as a finely divided mixture of two distinct phases: a contractile filament network and an aqueous solution. The material enclosing the cytoplasm (in most cases this will be the cell membrane) is modeled by assuming that the network and solution phases are enclosed within the walls of a rigid "reaction vessel."

The mathematical formulation of the reactive flow model involves a system of coupled, nonlinear, partial differential equations, together with boundary conditions. Unfortunately, analytical solution of these equations is possible only under very restrictive conditions. Consequently, in order to study the detailed behavior of the model, it is necessary to have recourse to large-scale numerical computations. In the appendix of this paper we present a summary of the differential equations, and we describe the details of a numerical method for their solution.

GLOSSARY

$\tilde{\theta}_n$	Network density at chemical equilibrium
T_{eq}	Relaxation time of network formation and breakdown
M_s	Solution shear viscosity
Λ_s	Solution dilatation viscosity
M_n	Network shear viscosity
Λ_n	Network dilatation viscosity
Φ	Network-solution drag coefficient
Ψ_F	Effective contractile stress
σ	Swelling number
L_x, L_y	Length of sides of reaction vessel
$\theta_n(0)$	Initial network density
STK*‡	Stick/No-stick index for network normal B.C.'s
SLS*	Slip/No-slip index for solution tangent B.C.'s
SLN*	Slip/No-slip index for network tangent B.C.'s
HYC*	Hydraulic conductivity for solution normal B.C.'s
PEX*	External pressure
DX and DY	Grid spacing along X and Y axes
dT	Time step
DEL	Parameter for adaptively controlling the size of the time step
EPS	Convergence parameter for time step iteration

BENCHMARK COMPUTATIONS

To evaluate the performance of our algorithm and the resulting implications for the reactive flow model, it is instructive to see the concrete results obtained for a family of illustrative cases. In choosing the starting point for such a series of computations, simplicity is desirable, but it is also desirable to model a situation where some experimental data are available. We consider the dynamics of a very simple sort of network that is capable of contraction but that does not undergo significant chemical breakdown and reformation. At zero time, we suppose that a reaction vessel is somehow filled by a perfectly uniform distribution of such a network, with mass density of about 1 mg/ml (the initial network volume fraction is taken to be 10^{-3}). We then "turn on" the contractile force. Table I lists the detailed parameters we shall adopt for this benchmark computation. The computation specified by Table I is

‡*T, B, L, R correspond to top, bottom, left-, and right-hand sides of the reaction vessel.

called Bench 0; descendants of Bench 0 are named Bench 1, Bench 2, etc.

The listings in Table I constitute a detailed account of all the information that must be specified at the start of a computation like Bench 0. This information is divided into two categories. The first is comprised of physical information about actual properties of the cytoplasm, the reaction vessel, and the initial conditions. The second is comprised of numerical information relevant to the accuracy with which the finite difference calculations are carried out. The significance of the various pieces of physical information has been discussed at length previously (see Dembo and Harlow, 1985). Numerical parameters and methods are discussed in the Appendix. For easy reference, the various symbols representing important physical and numerical parameters are listed and defined in the Glossary.

The reaction vessel in Bench 0 is of a very special sort. Most important, the vessel is two-dimensional, so that all motions of the network and solution are restricted to a plane. Within the plane of motion, the walls of the reaction vessel are a perfect square (10^{-2} cm on a side). All four walls of the vessel are of identical composition. The walls are slippery with respect to tangential sliding of both network and solution phases, they have no adhesive sites for preventing inward motions of the network, and they are impermeable to passage of the solution.

From the list of physical parameters in Table I, it can be seen that the parameters describing the chemical reaction of network formation and breakdown are chosen so as to ensure that these processes are negligible ($T_{eq} = \infty$ and $\tilde{\theta}_n = 0$). This is in accord with our supposition that the network in Bench 0 is unreactive. In choosing the other physical parameters in Table I, we have tried to make the most reasonable estimates we can, based on available experimental evidence (see Dembo and Harlow, 1985).

TABLE I
PARAMETER VALUES FOR BENCH 0

Size of reaction vessel*	$L_X = L_Y = 10^{-2}$ cm
Initial condition	$\theta_n(X,Y) = \theta_n(0) = 10^{-3}$ $1 \leq X \leq L_X$ $0 \leq Y \leq L_Y$
Boundary conditions§	STK‡ = −1, SLN‡ = +1, SLS‡ = +1, PEX‡ = 0, HYC‡ = 0
Physical parameters	(*a*) Chemical‖ $\hat{\theta}_n = 0$, $T_{eq} = \infty$
	(*b*) Rheological $M_s = 10^{-2}$ P, $\Lambda_s = 0$ P, $M_n = 10^5$ P, $\Lambda_n = 0$ P $\Phi = 10^8$ P/cm^2, $\Psi_F = 10^3$ dyn/cm^2, $\sigma = 0$
Numerical parameters	DX = DY = 6.25×10^{-5} cm DEL = 10^{-1} EPS = 10^{-3}

*This applies to the whole reaction vessel even though only one quadrant was calculated because of symmetry considerations.
§This applies to all boundaries; ‡ = T, B, L, and R. Boundaries are all no-stick, free-slip, impermeable, and support zero external pressure.
‖Note that the parameters are such that chemical reaction is negligible.

It is an exact analytic property of the equations describing the reactive flow model that symmetries in the initial conditions and boundary conditions will persist as symmetries in solutions of the equations. In extensive numerical trials we have found that our algorithm preserves this feature of the underlying model except under conditions where symmetric solutions are unstable. Even in the latter circumstances, symmetry breaking does not become noticeable until very long times as random roundoff errors become amplified. In Bench 0 the initial and boundary conditions have fourfold symmetry; rotation of the reaction vessel through any multiple of 90° leads to an identical configuration. Furthermore, numerical experiments demonstrate that the expected symmetric solutions are stable in the case of Bench 0. Thus, the dynamics in the entire reaction vessel can be observed by examining only one quadrant.

Fig. 1 *A* and *B* are computer-generated images illustrating the state of the first quadrant of the reaction vessel in Bench 0 at 2 min and 5 min after the start of contraction (time in seconds is noted on the top center of each figure). To show the detailed form of the pressure, density, and velocity fields at the two stages of the reaction, each figure is divided into four subplots.

The subplot in the upper left-hand corner of Fig. 1 *A* and *B* is a contour map of the natural logarithm of the normalized network volume fraction. The reference contour in this map is always taken at $\ln(\theta_n/\theta_0) = 0$. The scale parameter written in FORTRAN E-format to the left of the subplot indicates the value of the normalization constant, θ_0. Contour lines in this plot are spaced at half-log intervals: $\ln[\theta_n/\theta_0] = 0 \pm 0.5, \pm 1, \pm 1.5$, etc. This corresponds to $\theta_n = \theta_0$, $\theta_n = \theta_0 e^{\pm 0.5}$, $\theta_n = \theta_0 e^{\pm 1.0}$, $\theta_n = \theta_0 e^{\pm 1.5}$, etc.

In order to avoid the distracting clutter produced by contour lines corresponding to extremely low network densities, we usually delete lines at volume fractions below a certain cutoff. Unless otherwise noted, the cutoff is set at a level 100-fold smaller than θ_0.

As a graphical aid in locating the reference contour in black and white images, this line is slightly thickened. In color images, contour lines for $0.01\ \theta_0 < \theta_n < 0.1\ \theta_0$ are colored blue; lines in the interval $0.1\ \theta_0 < \theta_n < \theta_0$ are colored light blue; the middle contour, $\theta_n = \theta_0$, is colored yellow; lines for $\theta_0 < \theta_n < 10\ \theta_0$ are colored red; and lines such that $10\ \theta_0 < \theta_n < 1$ are colored magenta.

The subplot in the upper right-hand corner of Fig. 1 *A* and *B* gives a contour map of the effective pressure field at various points in the reaction vessel. The effective pressure is nearly the same as ordinary pressure but carries a correction for solvation interactions between the network and solution phase (Dembo, M., and F. Harlow, *Biophys. J.* 50:109–121).

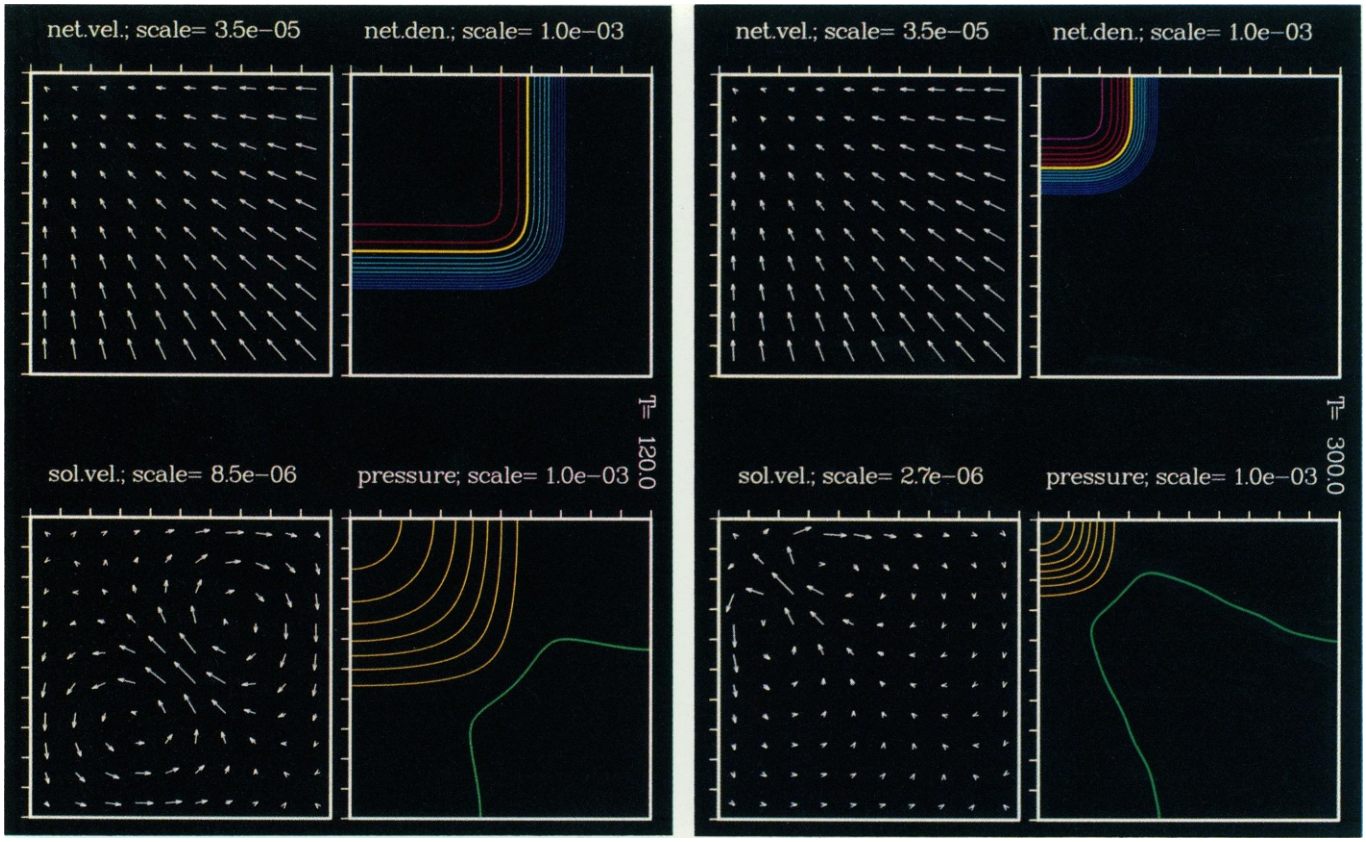

FIGURE 1 Nodal member of Benchmark series of computations (Bench 0). Detailed parameters are listed in Table I. (*A*) 2 min after start of reaction. (*B*) 5 min after start. At each time point the state of the reaction vessel is indicated by means of a network density contour map (top left), a pressure contour map (top right), a network velocity map (bottom left), and a solution velocity map (bottom right). Details required for quantitative interpretation of these subplots are described in the text.

In the case of the effective pressure field, the reference contour is always taken at a pressure of zero. The scale parameter written in FORTRAN E-format to the left of the subplot gives the spacing between contour levels in units of dynes/cm^2. As with the network density contour map, the reference pressure contour is thickened. Unlike the network density plot, negative pressure contours are blue, positive pressure contours are yellow, and the reference contour is colored green.

The subplot in the lower left-hand corner of Fig. 1 *A* and *B* is a vector map of the network velocity field. In producing this map, vectors are drawn emanating from 100 evenly spaced points throughout the reaction vessel. The direction of the arrowhead on each vector shows the direction of flow, and the length of the arrow is proportional to the speed of flow. The scale parameter, written in FORTRAN E-format on the left of the subplot, gives the speed in cm/s corresponding to a vector with length 1/10 the length of one of the walls of the reaction vessel.

The subplot in the lower right-hand corner of Fig. 1 *A* and *B* is a vector map of the solution velocity field. The format of the solution velocity map is the same as for the network velocity map except that the scale parameters on the two subplots are usually different.

Before we discuss the relationship of Bench 0 to experiments, it is necessary to know to what degree the numerical results really reflect true predictions of the underlying model. We must thus check to see whether the results of our calculations depend significantly on the numerical parameters in Table I. We must also check to see whether the numerical results are in accord with known analytical results.

We have already stated that the numerical solutions display the same symmetry-preserving property as the underlying analytic solutions. This property is quite general and would apply for any choice of physical parameters. A more specialized class of analytic results can be proved concerning the nature of the final equilibrium state of an unreactive contractile network. For example, consider a generalized version of Bench 0 where we start with arbitrary but uniform network and solution volume functions $\theta_n(0)$ and $\theta_s(0) = 1 - \theta_n(0)$, and where we include effects due to the swelling number σ.

If the contractile stress and the swelling number are both greater than zero, then there is a unique equilibrium value of the network density such that the solvation and contractile stresses counterbalance each other. This equilibrium network density is given by the nontrivial root of

the transcendental equation

$$\hat{\theta}_n + \sigma(\hat{\theta}_n + \ln(1 - \hat{\theta}_n)) = 0. \quad (1)$$

If the starting density of network is greater than $\hat{\theta}_n$, then the network will tend to expand. In the case of uniform initial density, expansion is prevented by the walls of the reaction vessel so that the final state will be the same as the initial state.

If the starting density of network is less than $\hat{\theta}_n$, then the network will tend to contract. Contraction will continue until an equilibrium is reached. In the final equilibrium, the interior of the reaction vessel must be sharply divided into one or more subregions that contain network and one or more subregions that are completely devoid of network. Furthermore, the kinetic energy at equilibrium will vanish and the effective pressure in the reaction vessel will be everywhere constant. The final network density in those subregions that contain network will be uniform and will equal $\hat{\theta}_n$.

A highly accurate algebraic approximation for $\hat{\theta}_n$ can be obtained by solving Eq. 1 using the method of Padé approximation. The result is

$$\hat{\theta}_n \sim (1 + 2\sigma)/(1 + \sigma)^2. \quad (2)$$

Eq. 2 has a maximum error of 7% in the range $0 < \sigma < \infty$.

For unreactive network, the total network mass must be the same in the initial and final states. Thus, if V_{final} is the final volume of the region (or regions) that contains network and if V_{vessel} is the total volume of the reaction vessel, then mass conservation implies that

$$\hat{\theta}_n V_{\text{final}} = \theta_n(0) V_{\text{vessel}}. \quad (3)$$

If we combine Eqs. 3 and 2, then we can compute the final extent of network contraction:

$$\frac{V_{\text{final}}}{V_{\text{vessel}}} \sim \frac{\theta_n(0)(1 + \sigma)^2}{(1 + 2\sigma)}. \quad (4)$$

We re-emphasize that Eqs. 1–4 only apply if the equilibrium state is not constrained by the walls of the reaction vessel, and, most importantly, only if the network is unreactive.

In most circumstances of biological interest, the starting density of network is highly dilute ($\theta_n(0) \lesssim 10^{-2}$). For such systems, Eq. 4 predicts a volume reduction in excess of 20-fold if the swelling number is <10. Thus, for sufficiently dilute networks, the reactive flow model predicts very extensive volume reductions.

Although negative swelling numbers do not seem to occur in real contractile networks, they are theoretically possible (see Dembo and Harlow, *Biophys. J.* 50:109–121). If the swelling number is negative and the effective contractile stress positive, the solvation and contraction stresses are additive and do not tend to counteract each other. Consequently, the reactive flow model predicts that network contraction will continue until the solution is completely squeezed out of the network containing subregions. This gives rise to a singular state in which there is complete separation for the two phases.

In numerical experiments with various swelling numbers and starting densities, our algorithm always approaches equilibrium solutions of the correct form. This includes cases where the network is expected to swell rather than contract and cases where phase separation is expected. For example, in the case of Bench 0, we have verified by direct integration that the total mass of network remains constant to within six significant figures at all stages of the contraction process. An additional check follows from the very sharp boundary of the central clump (remember that the light blue band in Fig. 1 *A* and *B* represents a 10-fold drop in network density). The sharpness of the fall-off of network density demonstrates that all the network material is contained within a subregion and that the surrounding portions of the reaction vessel are devoid of network.

To verify Eq. 2, it is necessary to carry computations out to very long times. When this precaution is taken, the approximate result is reproduced by our algorithm to within a few percent (data not shown).

One minor difficulty with computing equilibrium states occurs if the swelling number is negative or very close to zero (i.e., cases where phase separation is expected). In such computations an overflow error is encountered at a point where the maximum network density becomes very close to 1. Physically, this happens because the occurrence of phase separation contradicts a fundamental assumption of the reactive flow model (i.e., the assumption that the network and solution constitute a finely divided mixture).

We conclude that, at least for the case of unreactive networks, our numerical algorithm yields correct final states of the reactive flow model. This is certainly a desirable feature, but it does not have much bearing on the reliability of time-dependent aspects of various computations.

Another approach to testing the reliability of our numerical results comes from sequentially refining the spatial or temporal resolution. If the limit of fine resolution is the exact solution of the underlying model, then the sequence of calculations must be a Cauchy sequence with respect to some norm in function space. Thus, it may be possible to assess the accuracy of a computation by the degree to which successive refinements of the spatial or temporal grids fail to produce significant changes in results.

In the case of Bench 0, refinements in the temporal grid (i.e., the time step per cycle) have negligible effects on the results obtained (data not shown). The effects of a change in the spatial grid are illustrated by Fig. 2 *A* and *B*. As these figures show, there is very little effect on large scale features such as the size of the network mass, the speed of contraction, the pattern of solution flow, and the shape and spacing of the pressure contours. Nevertheless, the spatial resolution does have a significant effect on certain detailed aspects of the results.

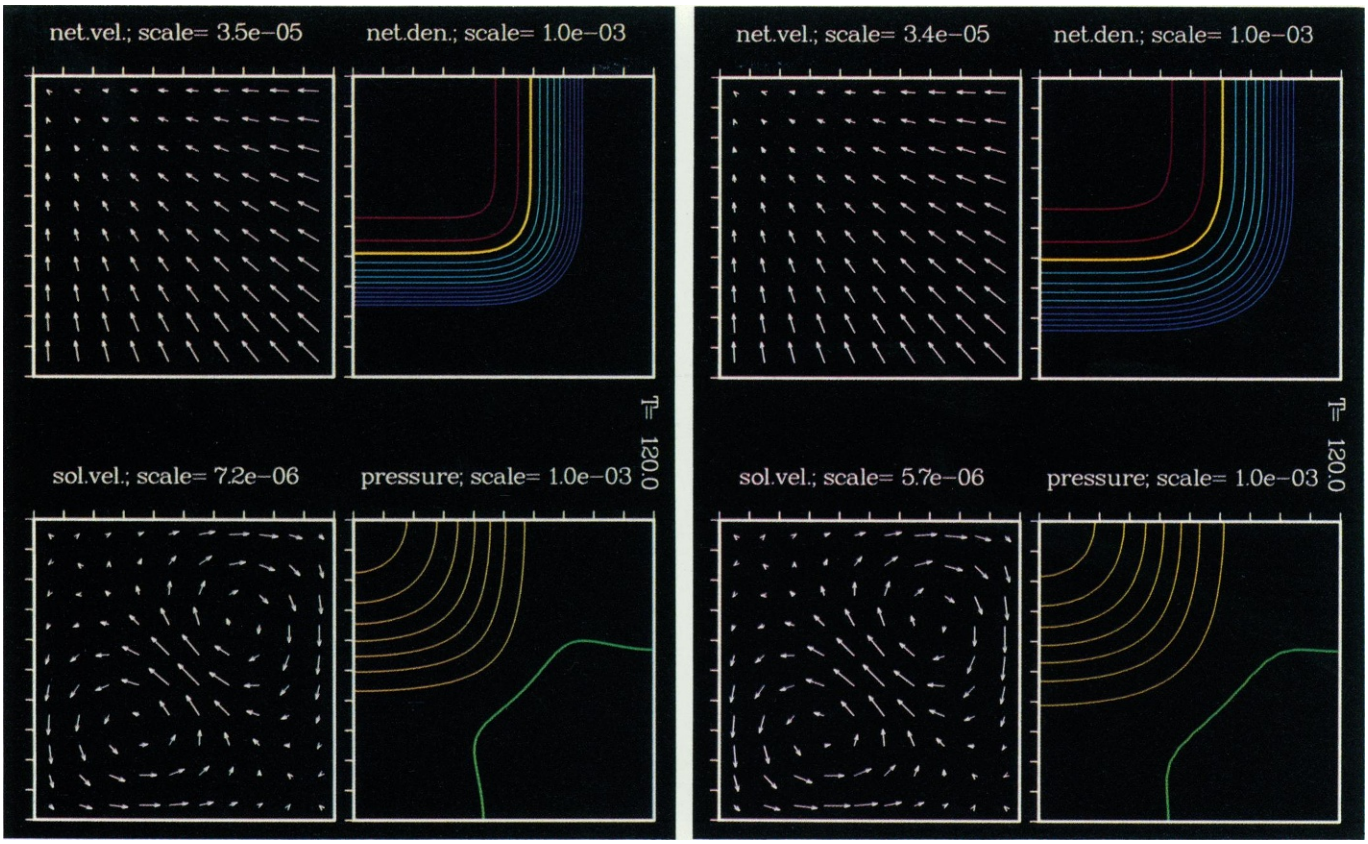

FIGURE 2 Effect of spatial grid on Bench 0. All parameters are the same as in Table I except that the spatial resolution is decreased. (*A*) Resolution decreased by a factor of 2 (DX = DY = 1.25×10^{-4} cm). (*B*) Resolution decreased by a factor of 4 (DX = DY = 2.5×10^{-4} cm). Decreasing spatial resolution results in smoothing out the sharp boundaries of the network mass. However, the basic size and shape of the network mass, as well as its velocity of contraction, are not much affected.

The main feature of Bench 0 that is strongly dependent on spatial resolution is the sharp transition zone or front that separates the central clump of network material from the remainder of the reaction vessel. In numerical trials, when the spatial resolution is decreased, the outermost (blue) contour lines are displaced farther outward, and the innermost (red) contour lines are displaced farther inward. In other words, the general size and shape of the network mass changes little, but the edge of the mass is smoothed out. These are not unexpected developments since numerical methods based on fixed Eulerian grids are notorious for their tendency to smooth out sharp fronts or shocks.

Decreases in spatial resolution also bring about several minor or secondary effects that result from the smoothing out of the edge of the network mass. One such effect is that the square corner of the network mass tends to become rounded as contraction proceeds. Thus, in low resolution computations, the network clump loses its original square outline and takes on a circular appearance more rapidly than in high resolution computations. Decreases in spatial resolution also result in small decreases in the speed of contraction (that is, smooth fronts move slower than sharp fronts). Thus in a 40×40 grid, the speed of contraction (as judged by the propagation of the yellow contour line) is about 5% slower than in an 80×80 grid (compare Figs. 1 *A* and 2 *A*). Other secondary effects include small displacements in the pressure field and in the speed of solution flow near the edge of the network clump.

So far we have been discussing the empirical interrelationships and limitations of the various solutions generated by our numerical techniques. Evidence of this kind allows us to have some confidence that, if carried out with sufficient accuracy, our numerical solutions will become reasonably close to true or exact solutions of the reactive flow model. It is thus possible to use our numerical techniques as a tool for comparing solutions of the reactive flow model with experimental observations.

Experimental Observations

An important body of experimental evidence on which the reactive flow model has direct bearing concerns the behavior of demembranated cytoplasm, partially purified cytoplasmic extracts, and reconstituted contractile systems constructed by mixing together purified and characterized cytoplasmic components. This type of experimental system offers considerable advantages since the size, shape, and composition of the reaction vessel, as well as the composition of the physiological medium and of the network itself, are controllable, at least to some degree.

Despite its relative simplicity, in some cases demembranated cytoplasm is capable of streaming, flaring, exhibiting periodic waves of contraction, and undergoing other complex motions that continue for very long times. In other cases, it is observed that after a transient burst of activity, the demembranated contractile network asymptotically approaches a state of mechanical equilibrium; that is, a state in which no further motion occurs. The reactive flow model is able to account for the existence of both these behaviors in terms of the relative importance of the chemical reaction of network formation and breakdown. If network material maintains rapid dynamic interchange with unpolymerized material, then a nonuniform steady state in which no network motion occurs is impossible. On the other hand, if network, once formed, is chemically stable, then a class of nonuniform states of mechanical equilibrium can be shown to exist (see preceding section).

Despite the importance of fully reactive networks, the dynamic complexity of such systems precludes an in-depth treatment in this paper. On the other hand, chemically stable networks seem to occur experimentally, and their behavior is both highly instructive and relatively simple to analyze. For our present discussion, we will assume that any experimental system where the network contracts and smoothly approaches a state of mechanical equilibrium can be regarded as a chemically stable network. By this criterion, major studies of chemically stable networks have been reported by Pollard (1976), Stossel and Hartwig (1976), Condeelis and Taylor (1977), Kane (1980), Stendahl and Stossel (1980), and Kane (1983). There are also many other reports.

The usual procedure for studying the contractile activity of unreactive networks starts with a solution containing the various components of the network in depolymerized form. On warming to room temperature, the polymerization reaction starts spontaneously. The progress of the reaction can be followed as a consequence of turbidity changes or by virtue of viscosity changes. For unknown reasons there is sometimes a natural lag between the completion of the polymerization reaction and the secondary contraction of the network. In other cases the contraction is inhibited during the network formation phase and is later initiated by addition of calcium ion or by some other means.

Once the contractile phase of the reaction starts, two major dynamical modes are observed. The first mode has been described (Pollard, 1976) as a violent reaction in which contractions tear the network apart (rending reaction). Rending is also described (Kane, 1983) as a failure of the network to "remain intact during contraction." The second mode is usually described as a progressive, overall contraction of the network with gradual expulsion of clear fluid (squeezing reaction). An additional mode of reaction, superprecipitation, has been observed in cases where the contractile phase starts before the polymerization phase is complete.

The final state of the rending reaction consists of a suspension containing small clumps of contracted material. The squeezing reaction ends with a single, small knot of contracted material floating in the reaction vessel. In either event, both the rending and squeezing reactions end with a state where no further motion occurs.

RESULTS

In reality, there is no such thing as a fully unreactive network; after all, the network has to form somehow. Thus to speak of an unreactive network implies that network formation and breakdown, after an initial transient, have slowed to the point where they are no longer important on the time scale of contraction. In the case of superprecipitation, this is a doubtful supposition since there seems to be overlap between the reactive phase of the network and the subsequent contractile phase. On the other hand, both the rending and squeezing modes pass through a phase where there is a more or less uniform network distribution that is constant in time. If we consider this as the starting point, then there is considerable basis for neglecting chemical reaction as far as the subsequent dynamics of the rending and squeezing modes are concerned.

However one justifies the comparison, there is a fundamental and obvious similarity between the results of computations such as Bench 0 and experimental observations of the squeezing reaction. This similarity is based primarily on only one dynamical feature of the reaction: the sharp, inwardly moving boundary between the turbid region containing network and the surrounding clear region of expelled fluid. It is also important that the moving boundary tends to maintain the original shape of the reaction vessel until very late in the contractile process (i.e., the network resists the tendency to "round up").

Given that the reactive flow model predicts solutions of general form observed in the squeezing reaction, it is a simple but rather unrewarding exercise to reproduce the velocity of the moving boundary in any particular experiment by adjustment of one or all of the many free parameters of the model.

A more cogent issue is whether or not the reactive flow model will allow the possibility of the network tearing itself into two or more pieces, and if so, how and why.

To examine this issue we have carried out a series of numerical experiments in which each of the physical parameters of Bench 0 was allowed to vary over several orders of magnitude while all other physical parameters, initial conditions, and boundary conditions remained fixed. Experimentally, rending is observed under conditions where extensive contraction is possible. Also, rendering occurs during the early stages of network contraction where the system is still far from final equilibrium. Accordingly, our parameter search was limited to cases where the ratio V_{final}/V_{vessel} was much less than 1 (see Eq.

4). Furthermore, computations were halted well before final equilibrium was reached. For computations that fall within this class, variations in the value of the swelling number have no detectable effect on results.

Variations of the two solution viscosities (M_s and Λ_s) between 10^{-2} and 10^{1} Poise, revealed no detectable effect on the scaling or on the dynamics of contraction. This means that, network viscosity dominates solution viscosity as long as the solution viscosities are less than ~ 10 poise.

The effect of variation in the starting density of network [$\theta_n(0)$] was somewhat similar to the effect of variation in the solution viscosities. The only effect of variations in $\theta_n(0)$ was an exactly proportional variation in the scale of the effective pressure field, of the solution velocity field, and of the network density field. The velocity and dynamics of the network motion were not detectably effected. These results are in accord with an interesting observation reported by Kane (1983). He observed that if the ratio of actin:myosin:actin-binding proteins was held fixed, then the rate of contraction in his system was independent of the total protein density.

Variation of the effective contractile stress (Ψ_F) always caused an exactly proportional change in the solution and network velocity fields and also in the scale of the effective pressure field. Thus, increasing or decreasing Ψ_F is like increasing or decreasing the speed of a motion picture projection. We conclude that the strength of contractile stresses is of little importance as far as the occurrence or nonoccurrence of rending is concerned.

Unexpectedly, we found that the network dilatation and shear viscosities, Λ_n and M_n, were largely interchangable in their effects. In other words, it is possible to define an effective lumped viscosity, $N_n \equiv \Lambda_n + M_n$, such that if N_n is held fixed, then we could not observe any significant changes due to variation of the ratio Λ_n/M_n. It was quite surprising to find that shear and dilatation apparently receive equal weight in determining the effective network viscosity for the two-dimensional contractions studied. Physically this result seems to occur because of the square shape of the contracting network mass. This shape forces the main loci for viscous dissipation of energy to fall along the diagonal of the reaction vessel. In the case of a perfectly radial or of a one-dimensional contraction, such concentration of stress does not occur, and the effective viscosity is given by $\Lambda_n + 2M_n$.

The interchangable nature of M_n and Λ_n is only an approximate relation. When the shear viscosity was more than 100 times smaller than the dilatation viscosity, marked changes in the shape of the contracting network mass were observed. These changes are apparently due to a tendency of the network to collapse inward along flat surfaces and to bulge outward at corners. The overall effect is to produce a spiny, or echinate morphology, of the type illustrated in Fig. 3. The number of arms to such echinate contractions increases if small perturbations are added to the initial network distribution. Thus, under low shear conditions, any small bumps and irregularities in the reaction vessel tend to become accentuated during contraction.

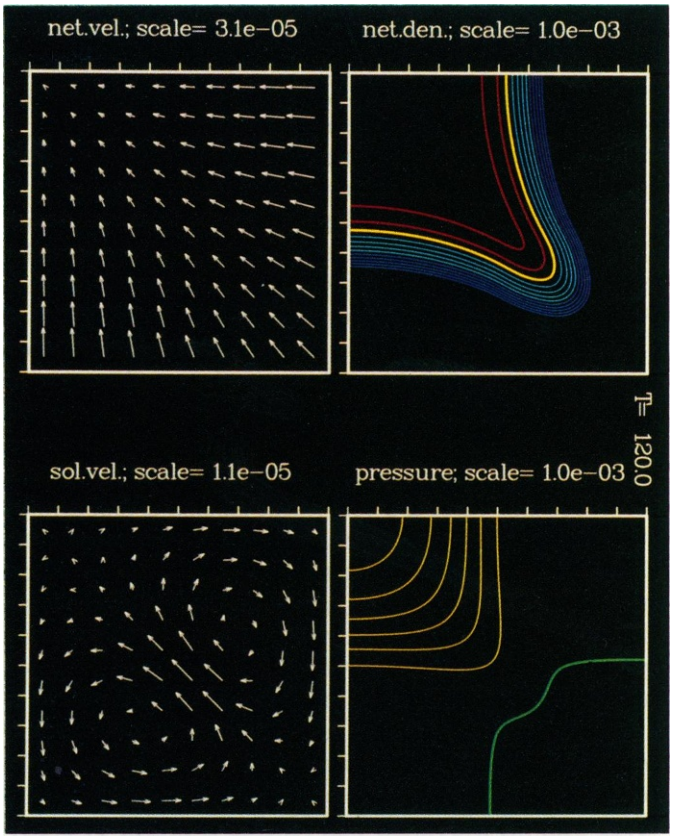

FIGURE 3 Squeezing reaction at low shear viscosity. Parameters are the same as in Table I except that the network dilatational viscosity is increased ($\Lambda_n = 9.99 \times 10^4$) and network shear viscosity decreased ($M_n = 10^3$). Note that the sum $M_n + \Lambda_n$ remains constant. Very low shear viscosity causes flat surfaces of the network mass to collapse inward while corners bulge outward. The result is a spiny or echinate contraction.

In contrast to the findings for σ, M_s, Λ_s, Ψ_F, $\theta_n(0)$, and the ratio Λ_n/M_n, variations in the effective network viscosity ($M_n + \Lambda_n$), the size of the reaction vessel (L_X), and the drag coefficient (Φ) greatly affected the dynamics of contraction. If these latter parameters were changed past a certain point, then the squeezing type reaction became unstable in favor of a mode where several pieces of network were formed.

Starting with the parameters in Table I, rending is achieved by increasing the values of L_X or Φ and by decreasing the value of $M_n + \Lambda_n$. Increasing L_X or Φ has the initial effect of simply slowing the time scale of the squeezing reaction. If L_X (or Φ) is increased further, there is an intermediate regime where the contracting network clump develops a number of localized nodules of high density. This leads the network mass in the final stages of contraction to resemble a "cluster of grapes." Nevertheless, in this stage the various nodules of high density remain

in contact and eventually fuse together. If L_X (or Φ) are increased even further, then there is actual breakup of the network into disconnected clumps which remain well separated. If $(M_n + \Lambda_n)$ is decreased, then the initial effect is to speed up the rate of the squeezing reaction. Nevertheless, beyond a certain point, decreasing $(M_n + \Lambda_n)$ leads to a "cluster of grapes" morphology and then to actual rending. Thus the dynamical effect of decreasing viscosity is the same as the effect produced by increasing drag coefficient or vessel size; the only difference is in the scaling.

Our various results on the factors that cause occurrence or nonoccurrence of the rending reaction can be summarized in terms of a single nondimensional parameter, the rending number, $\Phi L_X^2/(\Lambda_n + M_n)$. The cluster of grapes morphology occurs when the rending number has a value of ~100. This value is a convenient landmark that divides the regime of rending behavior from the regime of squeezing behavior. However, it should be realized that according to the reactive flow model, rending is simply the extreme limit of a continuous spectrum. Thus it does not seem possible, or appropriate, to designate a particular value of the rending number as the "threshold" for rending.

From the definition of the rending number, it can be seen that the contractility coefficient (Ψ_F) plays no role in determining whether or not rending occurs. This result is at odds with the hypothesis that rending is caused by overly strong or rapid contraction. In contrast to this sort of explanation, rending in the reactive flow model is due to inadequate cohesion of the network relative to the effects of solution drag; rending is not related to contractility.

Another important property of the rending number is its strong dependence on the size of the reaction vessel (L_X). This is not an unexpected finding since it simply means that a large mass of network will tend to tear more easily and into more pieces than a small mass. A final aspect of the rending number is its inverse dependence on a linear combination of the network viscosities, Λ_n and M_n.

Fig. 4 *A–D* illustrates a computation (Bench 3) with rending number equal to 1,000. All parameters in Bench 3 are the same as in Bench 0 except that the size of the reaction vessel (L_X) has been increased by a factor of 200.

The details of how the network tears itself apart in Bench 3 are quite typical. Fig. 4 *A* shows the network shortly after the start of the reaction. At this stage, the major dynamical effect of the high rending number can be seen in the velocity fields. In particular, the forces due to Stokes drag with the solvent are strong enough so that the network flows against the direction dictated by contractile forces in certain regions.

Fig. 4 *B* shows a somewhat later stage of the rending reaction. In Fig. 4 *B* it can be seen that a ring or cortex of high network density has developed along the periphery of the contracting network mass. There is also a series of parallel peaks and valleys of network density towards the center of the network mass. Thus, unlike the squeezing reaction, contraction at high rending numbers causes the interior of the network mass to fold and buckle into a sequence of concentric rings. The situation seems rather analogous to the formation of parallel mountain ranges by compression of continental plates.

In Fig. 4 *C* the outermost or primary ring of high network density has greatly increased in mass and has substantially separated from the secondary ring. Simultaneous circumferential contractions in the primary ring cause it to develop several separate peaks.

In Fig. 4 *D* the primary ring has completely split into a number of separate clumps of contracting material. Meanwhile, further contraction of the central network mass has caused the secondary ring to grow in density and separate from the central network mass. Note also, that one of the pieces from the primary ring has been pulled into the secondary ring. In Fig. 4 *E* the secondary ring begins to undergo circumferential fission.

For the parameters in Bench 3 we can detect only three rounds of division before the various pieces formed are all too small to undergo further fission. The larger the value of the rending number, the larger the number of sequential

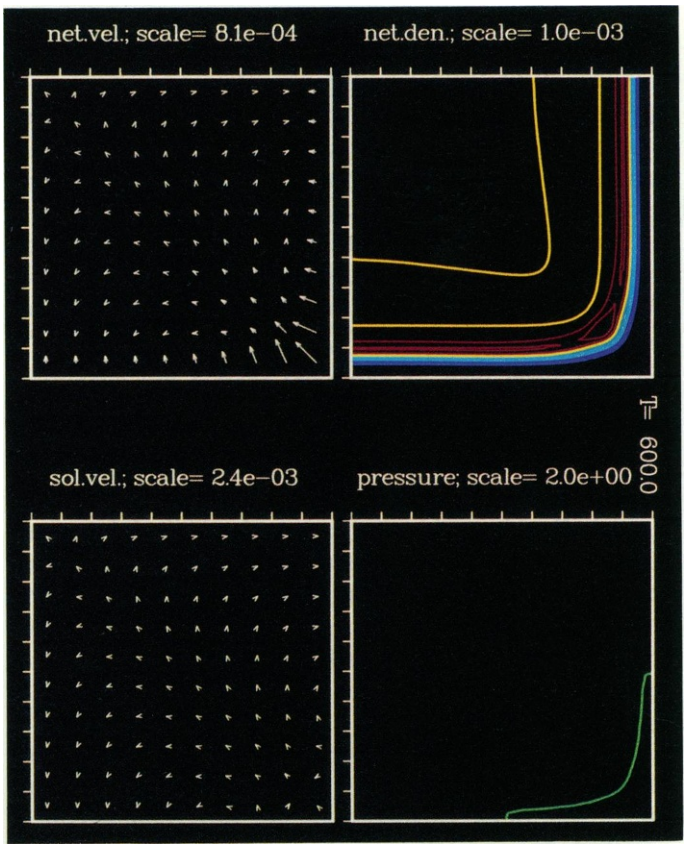

FIGURE 4 If the rending number is much greater than 100, the network tears itself into a number of separate pieces during contraction. (*A*) thru (*E*) represent various stages in the process of rending for a computation with rending number of 1,000. All parameters in this computation are the same as Table I, except that the size of the reaction vessel and of the grid cells are increased by a factor of 200 ($L_X = L_Y = 2$ cm, DX = DY = 1.25×10^2). (*A*) Development of primary cortex. (*B*) Separation of primary cortex. (*C*) Circumferential splitting of primary cortex. (*D*) Development of secondary cortex. (*E*) Splitting of secondary cortex.

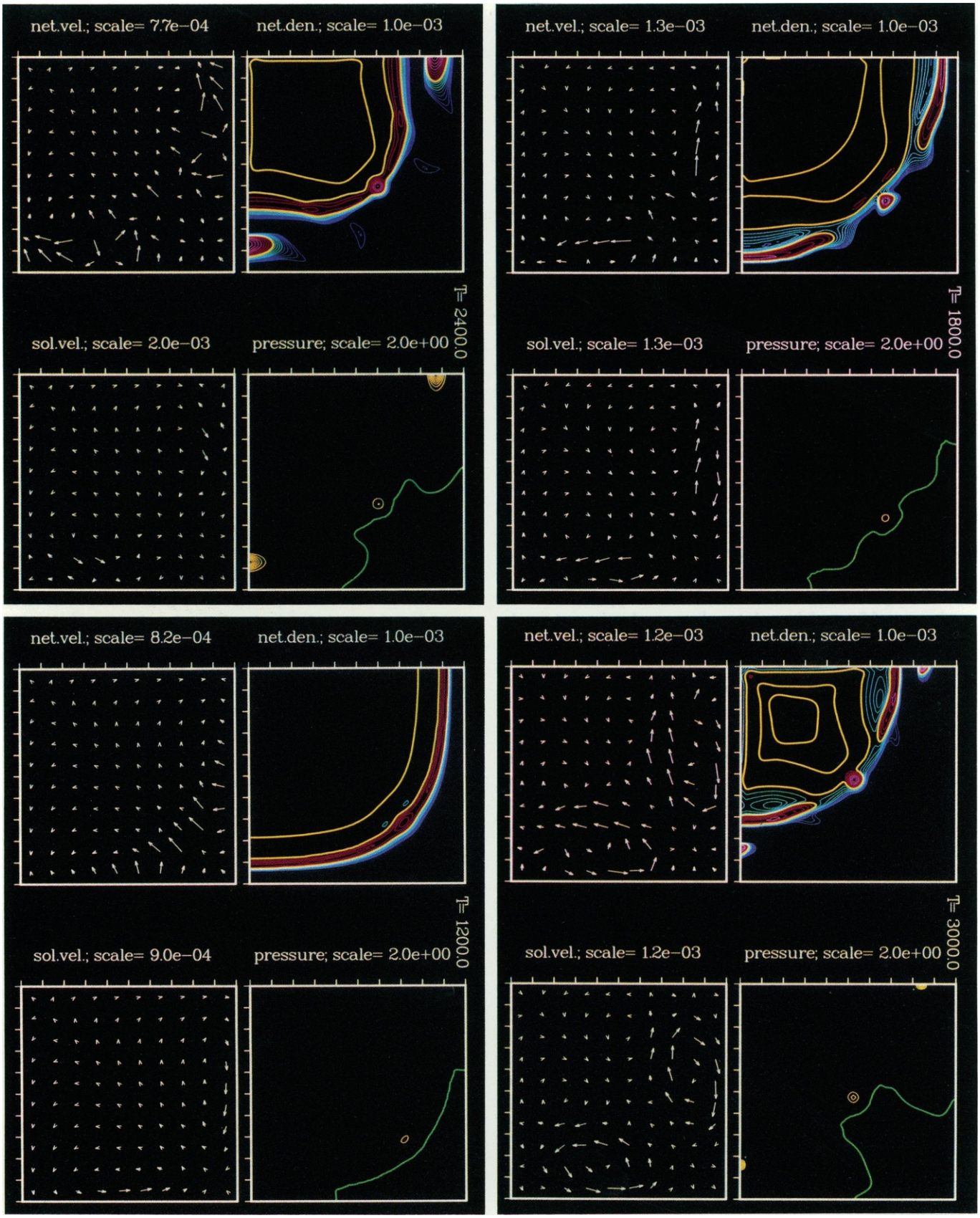

FIGURE 4 Continued

divisions and the greater the number of pieces formed at each stage. Furthermore, if the rending number is increased, then additional dynamical processes contribute to the breakup of the network mass. These include the formation of interconnecting cavities or vacuoles (like Swiss cheese). There are also large scale fission events wherein the contractile stresses cause the network mass to spontaneously divide into two (or four) equal pieces. Unfortunately, if the rending number is very large, then it is impossible to be precise about the exact number of pieces that will ultimately be formed. This is because the spatial resolution required to follow each of the increasingly small pieces exceeds the capacity of the computer. Nevertheless, it seems clear that for larger and larger values of the rending number, the process of repeated fission events would produce a geometric explosion in the number of pieces.

Pollard (1976) has shown that the transition from the squeezing mode to the rending mode in *Acanthamoeba* extracts can be caused by addition of small amounts of calcium cloride. At low levels of added calcium ($\lesssim 10^{-8}$ M) there is initial formation of stable gel; and after a variable lag, the squeezing reaction occurs with a slow time scale ($\gtrsim 1$ h). At higher levels of added calcium ($\gtrsim 10^{-7}$ M), initial formation of stable gel still occurs; but after the lag phase, there is occurrence of the rending reaction with more rapid time scale (~ 10 min).

To explain Pollard's results, we must suppose that in the absence of free calcium the rending number is on the order of 10^2 or less and that when calcium is added, the rending number increases to a value of more than 10^3. Since the size of the reaction vessel is not changed by adding calcium and since the drag coefficient is also very insensitive to chemical perturbation (see Dembo and Harlow, 1985), such a large increase in the rending number must be caused by a major decrease in the effective network viscosity $\Lambda_n + M_n$. In light of the known calcium dependence of enzymes such as gelsolin, such an effect of calcium is plausible. Unfortunately, direct measurements of viscosity were not reported by Pollard, so this explanation must remain hypothetical. It is interesting, however, that a decrease in viscosity would explain the marked difference in the time scale of rending and squeezing without having to invoke any other effect of calcium.

Kane (1983) observed a transition from the squeezing to the rending mode when the content of actin-binding protein in his preparations was decreased. In this case it is less ambiguous to directly conclude that the squeezing to rending transition is caused by changing the network viscosity and not by changing the contractility or some other parameter. This is in accord with our formulation of the rending number. In further support of this formulation, Kane showed that changes in myosin content caused changes in the time scale of contraction but did not change the mode.

CONCLUSION

Numerical techniques can be powerful tools for analyzing and understanding a complex physical system. However, it is easy to be misled into believing without question that the results of a computation are synonymous with the "true," or exact, solutions of the underlying model. In the present study we have tried to provide some basis for such belief by comparing our numerical results with known analytical properties and by checking the numerical results for internal consistency. Our tests have revealed only some standard artifacts associated with spatial resolution. These numerical artifacts apparently are not so severe as to affect the utility of the computations except with regard to very fine details. Nevertheless, certain artifacts may have gone undetected by our tests.

Assuming that our numerical results are reasonably close to true solutions of the reactive flow model, we can proceed to use the computer as a tool for analysis of the model itself. Even for the simple case discussed in this paper, the numerical approach has revealed behavior buried in the equations that would be extremely difficult to deduce by any other means (for example, the existence of the rending mode).

An important problem with numerical methodology as a tool in mathematics arises from a philosophical issue. We are able to carry out many particular computations using the reactive flow model, but at some point we are forced to stop focusing on individual cases and make some inductive statement about our overall results. Thus our understanding of many aspects of the reactive flow model is not based on traditional norms of mathematical certainty and rigor. Rather, we are forced to analyze a mathematical model in the same way that an experimentalist analyzes a real physical or chemical system. Our main advantage is that we are omnipotent with respect to our control of all input variables in the system, and we have complete reproducibility of results. Still, in the end, common sense joins with mathematical ingenuity as an indispensable element.

In the present study, the illustrative computations we have carried out were simplified and were largely restricted to the case of an unreactive network contained in a two-dimensional reaction vessel with square shape and with particular boundary conditions and particular initial conditions. After much experience, we feel that we understand in some detail the behavior of the model for this specialized case. However, extreme caution must be exercised when extending our results to more complex situations. For example, if the starting distribution of network is nonuniform, then it is reasonable to suppose that rending will occur preferentially along contours of low network density. Thus the landmark value of the rending number that we find in the present study, as well as the overall pattern of the reaction, are dependent on the initial conditions. Also, it is highly probable that the rending reaction

will be substantially different if the walls of the reaction vessel are sticky or if motion occurs in three dimensions.

An important factor left out of the computations we have presented in this study has been the chemical reaction of network formation and breakdown. When this factor is included, many of the dynamical properties we have described are likely to change. For example, states of nonuniform mechanical equilibrium no longer exist. As another example, increases and decreases in the effective contractile stress in fully reactive networks cannot be accounted for by renormalization of the pressure field and the time scale. Thus it is dangerous to generalize our findings to the case of fully reactive networks.

Understanding of the purely mathematical behavior of the reactive flow model is of considerable value in its evaluation. Also useful are comparisons of calculations and experimental results. In this regard, the reactive flow model is able to explain the two major dynamical modes that are observed in studies of simple, chemically stable contractile networks. The model is also able to give some account of the observed dynamical and scaling effects caused by changes in initial density, myosin content, content of actin-binding protein, and calcium concentration.

One area in which it is difficult to interpret experimental results concerns the endpoint of the squeezing reaction. As we have discussed previously, unless the swelling number is very large, extensive volume reductions are predicted for dilute networks (see Eq. 4). In the case of the squeezing reaction, some investigators have reported final volume reductions of up to 100-fold, while others report that contraction stops after only a 10-fold reduction in volume. The starting network density in all experimental studies was on the order of 1 mg/ml (i.e., $\theta_n(0) \sim 10^{-3}$). Thus these results indicate that the swelling number is greater than 10.

Superficially, the occurrence of a large swelling number suggests that solvation stresses are very important (see Eq. 9c, Dembo, M., and F. Harlow, manuscript submitted for publication). Unfortunately, this explanation seems overly simplistic. In particular, if the solvation coefficient were large, then maneuvers that cause a drop in contractile activity (e.g., removal of calcium) should cause re-expansion of contracted network clumps. Such re-expansion of contracted networks has never been reported.

A large value of the swelling number could also occur because of a very sharp decline in contractile stress as the network density increases (i.e., $\Psi'(0)/\Psi(0)$ is very much less than -1). This would indicate a failure of the actin-myosin interaction to produce tension at high network densities.

Incomplete contraction could also occur because of factors that are not accounted for in the reactive flow model. One such explanation for incomplete contraction involves time-dependent effects such as loss of contractile activity due to exhaustion of ATP pools or due to loss of myosin ATPase activity because of denaturing side reactions. Another explanation is that the very process of contraction somehow induces a gradual or sudden increase in network viscosity (i.e., gelation).

Although it may be necessary to incorporate additional effects, the reactive flow model is in substantial accord with the available observations on unreactive networks. Of course, other models might also explain the available observations equally well. Nevertheless, it is important to realize that the ability of models to produce both squeezing and rending modes of contraction is not expected to be universal. For example, any continuum model containing a component of true elastic or viscoelastic behavior cannot give rise to alterations in topological connectivity from the initial conditions (the potential energy associated with such a change is infinite). On the other hand, fluids are notorious for their ability to undergo topological changes (consider the dynamics of a splash or of cavitation).

We feel that the demonstrated ability of biological contractile networks to undergo changes in topological connectivity is quite fundamental. After all, what else is involved in cell division or phagocytosis? Thus, despite the popularity of the "gel" concept in describing contractile networks, it seems doubtful that such a concept is valid, at least in the regime of large deformation. The importance of network fluidity is also supported by independent lines of evidence (Condeelis and Taylor, 1977) and has been previously discussed as the solation-contraction-coupling hypothesis (Hellewell and Taylor, 1979).

APPENDIX: NUMERICAL METHODS

Our purpose in this appendix is to set forth in some detail an algorithm we have developed for solving the reactive flow model in the special case of two-dimensional rectangular geometries when all coefficients are constants. We start by rewriting the equations of the model in a form appropriate for this restricted class of problems.

Let L_X and L_Y be the lengths of the two sides of a rectangular reaction vessel, and let Cartesian coordinates be defined such that the interior of the reaction vessel is given by a set of points $\{\mathbf{R} = (X, Y) | 0 \le X \le L_X, 0 \le Y \le L_Y\}$. We express the velocity fields of the network and solution phases in terms of X and Y components by $\Omega_n(\mathbf{R}, t) = [U_n(\mathbf{R}, t), V_n(\mathbf{R}, t)]$ and $\Omega_s(\mathbf{R}, t) = [U_s(\mathbf{R}, t), V_s(\mathbf{R}, t)]$, respectively. The network and solution volume fractions, at various points in the reaction vessel, are given by continuous functions of position and time, $\theta_n(\mathbf{R}, t)$ and $\theta_s(\mathbf{R}, t)$, respectively. We define $P_F(\mathbf{R}, t)$ to be the mechano-chemical potential per unit volume of the solution phase $P_F \equiv P_s + \Upsilon \ln(\theta_s)$, where P_s is the solution pressure, and Υ is the solvation coefficient. We refer to P_F as the effective pressure.

According to the reactive flow model, the seven field variables—θ_n, θ_s, P_F, U_n, U_s, V_n, and V_s—must satisfy the following system of equations at all positions within the reaction vessel and at all positive times.

(*a*) The excluded volume relation

$$0 = \mathrm{FXV}(\mathbf{R}, t) = \theta_n + \theta_s - 1. \tag{A1}$$

(*b*) Conservation of volume

$$0 = \mathrm{FVC}(\mathbf{R}, t) = \partial_X[\theta_s U_s + \theta_n U_n] + \partial_Y[\theta_s V_s + \theta_n V_n]. \tag{A2}$$

(*c*) Conservation of network mass

$$0 = \mathrm{FNC}(\mathbf{R}, t) = -\partial_t\theta_n + \partial_X[\theta_n U_n] + \partial_Y[\theta_n V_n] + (\tilde{\theta}_n - \theta_n)T_{eq}^{-1}. \quad \text{(A3)}$$

(*d*) Conservation of X component of solution momentum

$$0 = \mathrm{FUS}(\mathbf{R}, t) = \partial_X\Lambda_s\theta_s[\partial_X U_s + \partial_Y V_s] + 2\partial_X M_s\theta_s\partial_X U_s + \partial_Y M_s\theta_s[\partial_Y U_s + \partial_X V_s] - \theta_s\partial_X P_F + \Phi\theta_s\theta_n(U_n - U_s). \quad \text{(A4)}$$

(*e*) Conservation of X component of network momentum

$$0 = \mathrm{FUN}(\mathbf{R}, t) = \partial_X\Lambda_n\theta_n[\partial_X U_n + \partial_Y V_n] + 2\partial_X M_n\theta_n\partial_X U_n + \partial_Y M_n\theta_n[\partial_Y U_n + \partial_X V_n] - \theta_n\partial_X P_F + \Phi\theta_n\theta_s(U_s - U_n) + \Psi_F(1 - \sigma\theta_n/\theta_s)\partial_X\theta_n. \quad \text{(A5)}$$

(*f*) Conservation of Y component of solution momentum

$$0 = \mathrm{FVS}(\mathbf{R}, t) = \partial_Y\Lambda_s\theta_s[\partial_Y V_s + \partial_X U_s] + 2\partial_Y M_s\theta_s\partial_Y V_s + \partial_X M_s\theta_s[\partial_X V_s + \partial_Y U_s] - \theta_s\partial_Y P_F + \Phi\theta_s\theta_n(V_n - V_s). \quad \text{(A6)}$$

(*g*) Conservation of Y component of network momentum

$$0 = \mathrm{FVN}(\mathbf{R}, t) = \partial_Y\Lambda_n\theta_n[\partial_Y V_n + \partial_X U_n] + 2\partial_Y M_n\theta_n\partial_Y V_n + \partial_X M_n\theta_n[\partial_X V_n + \partial_Y U_n] - \theta_n\partial_Y P_F + \Phi\theta_s\theta_n(V_s - V_n) + \Psi_F(1 - \sigma\theta_n/\theta_s)\partial_Y\theta_n. \quad \text{(A7)}$$

For easy reference, the nine parameters appearing in Eqs. A1–A7 are listed and defined in Table II.

In addition to Eqs. 1–7, the reactive flow model requires specification of boundary conditions at the walls of the reaction vessel. In order to illustrate the possibilities, let us assume that each of the four walls of the reaction vessel may be composed of a different kind of material, but that within a given wall the material properties of the boundary remain constant. Under this assumption, we can describe the boundary conditions on the top wall of the reaction vessel in terms of five quantities:

SLST = +1 if the top wall is a free-slip boundary with respect to the solution.
= −1 if the top wall is a no-slip boundary with respect to the solution.

SLNT = +1 if the top wall is a free-slip boundary with respect to network.
= −1 if the top wall is a no-slip boundary with respect to network.

STKT = +1 if the top wall is a "stick" boundary with respect to network.
= −1 if the top wall is a no-stick boundary with respect to network.

HYCT = Hydraulic conductivity of the top wall with respect to solution.

PEXT = External pressure on the top boundary.

In terms of these five descriptive parameters, the boundary conditions on the top wall of the reaction vessel are:

(*a*) Solution tangent velocity

$$[1 + \mathrm{SLST}]\partial_Y U_s + [1 - \mathrm{SLST}]U_s = 0,$$

(*b*) Network tangent velocity

$$[1 + \mathrm{SLNT}]\partial_Y U_n + [1 - \mathrm{SLNT}]U_n = 0,$$

(*c*) Solution normal velocity

$$V_s = \mathrm{HYCT}[P_F - \mathrm{PEXT}],$$

(*d*) Network normal velocity

$$(1 + \mathrm{STKT})V_n + (1 - \mathrm{STKT})(\Lambda_n\partial_X U_n + (\Lambda_n + 2M_n)\partial_Y V_n + \Psi_F) = 0,$$

(*e*) Network density

$$(1 + \mathrm{STKT})\partial_Y\theta_n + (1 - \mathrm{STKT})\theta_n = 0. \quad \text{(A8)}$$

The boundary conditions on the remaining three walls of the reaction vessel are specified in an analogous fashion.

Formulation in Terms of Finite Differences

For purposes of finite difference computations we divide the reaction vessel into a number of rectangular cells. To increase flexibility we will allow the number of cells along the X direction, NX, to be different from the number along the Y direction, NY. The spacing between cells in the X and Y directions are DX = L_X/NX and DY = L_Y/NY, respectively.

It is convenient to denote the various grid cells that fall within the reaction vessel by ordered pairs of integers (j, k) where $2 \le j \le \mathrm{NX} + 1$ and $2 \le k \le \mathrm{NY} + 1$. This numbering system leaves a row of cells, k = 1, $2 \le j \le \mathrm{NX} + 1$ underneath the bottom wall of the reaction vessel, and a similar column of cells, $j = 1$, $2 \le \mathrm{k} \le \mathrm{NY} + 1$ to the left of the left wall. These seemingly superfluous cells, together with the analogous row and columns adjacent to the top and right walls, are referred to as boundary cells. They have no physical significance, but their inclusion greatly facilitates the correct imposition of the boundary conditions.

If dT is the size of a small time interval, then for each pair of indices (j, k) we will define discrete arrays

TNO(j, k) ≡ Value of θ_n in center of cell (j, k) at time T

TN(j, k) ≡ Value of θ_n in center of cell (j, k) at time $T + \frac{1}{2}$ dT

TS(j, k) ≡ Value of θ_s in center of cell (j, k) at time $T +$ dT

PF(j, k) ≡ Value of P_F in center of cell (j, k) at time $T +$ dT

US(j, k) ≡ Value of U_s at the center of the right edge of cell (j, k) at time $T +$ dT

UN(j, k) ≡ Value of U_n at the center of the right edge of cell (j, k) at time $T +$ dT

VS(j, k) ≡ Value of V_s at the center of the top edge of cell (j, k) at time $T +$ dT

VN(j, k) ≡ Value of V_n at the center of the top edge of cell (j, k) at time $T +$ dT.

In terms of these arrays, the finite difference form of the excluded volume relation at cell (j, k) becomes

$$0 = \mathrm{FXV}(j, k) = \mathrm{TN}(j, k) + \mathrm{TS}(j, k) - 1. \quad \text{(A9)}$$

In discretizing the expressions for conservation of mass and volume, we will make use of so-called upstream differencing. In order to facilitate upstream differencing, it is convenient to introduce the following so-called "stream" averages to approximate the volume fractions on the various edges (top, bottom, left, and right) of cell (j, k):

$$\mathrm{TNT} = \tfrac{1}{2}[(\mathrm{ZNT} + 1)\mathrm{TN}(j, k) + (1 - \mathrm{ZNT})\mathrm{TN}(j, k + 1)]$$

$$\text{TNB} = \tfrac{1}{2}[(\text{ZNB}+1)\text{TN}(j,k-1) + (1-\text{ZNB})\text{TN}(j,k)]$$
$$\text{TNL} = \tfrac{1}{2}[(\text{ZNL}+1)\text{TN}(j-1,k) + (1-\text{ZNL})\text{TN}(j,k)]$$
$$\text{TNR} = \tfrac{1}{2}[(\text{ZNR}+1)\text{TN}(j,k) + (1-\text{ZNR})\text{TN}(j+1,k)]$$
$$\text{TST} = \tfrac{1}{2}[(\text{ZST}+1)\text{TS}(j,k) + (1-\text{ZST})\text{TS}(j,k+1)]$$
$$\text{TSB} = \tfrac{1}{2}[(\text{ZSB}+1)\text{TS}(j,k-1) + (1-\text{ZSB})\text{TS}(j,k)]$$
$$\text{TSL} = \tfrac{1}{2}[(\text{ZSL}+1)\text{TS}(j-1,k) + (1-\text{ZSL})\text{TS}(j,k)]$$
$$\text{TSR} = \tfrac{1}{2}[(\text{ZSR}+1)\text{TS}(j,k) + (1-\text{ZSR})\text{TS}(j+1,k)]$$

where

$$\text{ZNT} = \text{SIGN}[1, \text{VN}(j,k)];\ \text{ZST} = \text{SIGN}[1, \text{VS}(j,k)]$$
$$\text{ZNB} = \text{SIGN}[1, \text{VN}(j,k-1)];\quad \text{ZSB} = \text{SIGN}[1, \text{VS}(j,k-1)]$$
$$\text{ZNL} = \text{SIGN}[1, \text{UN}(j-1,k)];\quad \text{ZSL} = \text{SIGN}[1, \text{US}(j-1,k)]$$
$$\text{ZNR} = \text{SIGN}[1, \text{UN}(j,k)];\ \text{and}\quad \text{ZSR} = \text{SIGN}[1, \text{US}(j,k)].^{1}$$

In terms of the stream averages, the finite difference expressions for volume and mass conservation at the center of cell (j, k) are:

$$0 = \text{FCV}(j,k) = \frac{\text{UN}(j,k)\text{TNR} - \text{UN}(j-1,k)\text{TNL}}{\text{DX}} + \frac{\text{US}(j,k)\text{TSR} - \text{US}(j-1,k)\text{TSL}}{\text{DX}} + \frac{\text{VN}(j,k)\text{TNT} - \text{VN}(j,k-1)\text{TNB}}{\text{DY}} + \frac{\text{VS}(j,k)\text{TST} - \text{VS}(j,k-1)\text{TSB}}{\text{DY}} \tag{A10}$$

and

$$0 = \text{FCN}(j,k) = -\frac{\text{TN}(j,k) - \text{TNO}(j,k)}{dT} - \frac{\text{UN}(j,k)\text{TNR} - \text{UN}(j-1,k)\text{TNL}}{\text{DX}} - \frac{\text{VN}(j,k)\text{TNT} - \text{VN}(j,k-1)\text{TNB}}{\text{DY}} + [\tilde{\theta}_n - \text{TN}(j,k)]T_{eq}^{-1}. \tag{A11}$$

In discretizing the equations of X-momentum conservation, it is convenient to introduce some additional notation. Thus we define the right-hand "face averages" of cell (j, k) as

$$\text{TSRF} \equiv \sqrt{\text{TS}(j,k)\text{TS}(j+1,k)}\ \text{TNRF} = 1 - \text{TRSF}.$$

Use of these rather unusual expressions for the face averages is necessary in order to ensure attainment of proper equilibrium solutions.

We also define the so-called top-right and bottom-right "corner averages" of cell (j, k):

$$\text{TNTC} \equiv \min[\text{TN}(j,k), \text{TN}(j+1,k), \text{TN}(j,k+1), \text{TN}(j+1,k+1)]$$
$$\text{TNBC} \equiv \min[\text{TN}(j,k-1), \text{TN}(j+1,k-1), \text{TN}(j,k), \text{TN}(j,k+1)]$$
$$\text{TSTC} \equiv \min[\text{TS}(j,k), \text{TS}(j+1,k), \text{TS}(j,k+1), \text{TS}(j+1,k+1)]$$
$$\text{TSBC} \equiv \min[\text{TS}(j,k-1), \text{TS}(j+1,k-1), \text{TS}(j,k), \text{TS}(j,k+1)]$$

In terms of these quantities, the finite difference forms of Eq. A4 and A5 are

$$\begin{aligned} 0 = \text{FUS}(j,k) = {} & \frac{\Lambda_s + 2M_s}{\text{DX}^2} \cdot \{\text{TS}(j+1,k)[\text{US}(j+1,k) - \text{US}(j,k)] - \text{TS}(j,k)[\text{US}(j,k) - \text{US}(j-1,k)]\} \\ & + \frac{\Lambda_s}{\text{DXDY}}\{\text{TS}(j+1,k)[\text{VS}(j+1,k) - \text{VS}(j+1,k-1)] - \text{TS}(j,k)[\text{VS}(j,k) - \text{VS}(j,k-1)]\} \\ & + \frac{M_s}{\text{DY}^2}\{\text{TSTC}[\text{US}(j,k+1) - \text{US}(j,k)] - \text{TSBC}[\text{US}(j,k) - \text{US}(j,k-1)]\} \\ & + \frac{M_s}{\text{DXDY}}\{\text{TSTC}[\text{VS}(j+1,k) - \text{VS}(j,k)] - \text{TSBC}[\text{VS}(j+1,k-1) - \text{VS}(j,k-1)]\} \\ & - \Phi(\text{TSRF})(\text{TNRF})[\text{US}(j,k) - \text{UN}(j,k)] - (\text{TSRF}/\text{DX})[\text{PF}(j+1,k) - \text{PF}(j,k)] \end{aligned} \tag{A12}$$

and

$$\begin{aligned} 0 = \text{FUN}(j,k) = {} & \frac{\Lambda_n + 2M_n}{\text{DX}^2} \cdot \{\text{TN}(j+1,k)[\text{UN}(j+1,k) - \text{UN}(j,k)] - \text{TN}(j,k)[\text{UN}(j,k) - \text{UN}(j-1,k)]\} \\ & + \frac{\Lambda_n}{\text{DXDY}}\{\text{TN}(j+1,k)[\text{VN}(j+1,k) - \text{VN}(j+1,k-1)] - \text{TN}(j,k)[\text{VN}(j,k) - \text{VN}(j,k-1)]\} \\ & + \frac{M_n}{\text{DY}^2}\{\text{TNTC}[\text{UN}(j,k+1) - \text{UN}(j,k)] - \text{TNBC}[\text{UN}(j,k) - \text{UN}(j,k-1)]\} \\ & + \frac{M_n}{\text{DXDY}}\{\text{TNTC}[\text{VN}(j+1,k) - \text{VN}(j,k)] - \text{TNBC}[\text{VN}(j+1,k-1) - \text{VN}(j,k-1)]\} \\ & - \Phi(\text{TNRF})(\text{TSRF})[\text{UN}(j,k) - \text{US}(j,k)] - (\text{TNRF}/\text{DX})[\text{PF}(j+1,k) - \text{PF}(j,k)] \\ & + \Psi_F(1 - \sigma\text{TNRF}/\text{TSRF})/\text{DX})[\text{TN}(j+1,k) - \text{TN}(j,k)]. \end{aligned} \tag{A13}$$

[1] SIGN(a, b) is a standard function for most FORTRAN compilers. The mathematical definition is: SIGN$(a, b) = ab/|b|$.

The finite difference equations for conservation of Y momentum are obtained by interchange of the roles of the X and Y axes in Eqs. A11 and A12.

The differencing schemes for FUN(j, k) and FUS(j, k) are centered about the right-hand edge of cell (j, k), whereas the corresponding schemes for conservation of Y-momentum (FVS$[j, k]$ and FVN$[j, k]$) are centered at the top edge of cell (j, k). Because the momentum conservations equations hold only in the interior of the reaction vessel, FVN(j, k) and FVS(j, k) do not hold unless the values of j and k are such that the top of cell (j, k) is in the interior of the reaction vessel. Similarly, FUN(j, k) and FUS(j, k) do not hold if the right-hand edge of cell (j, k) is on the boundary or outside the boundary. The differencing schemes for FXV(j, k), FCV(j, k), and FCN(j, k) are centered at the midpoint of cell (j, k). Thus, the equations do not hold if cell (j, k) is a boundary cell.

Additional difference equations that hold only along the boundaries of the reaction vessel are derived from the boundary conditions. For example, along the top wall of the reaction vessel, the boundary conditions lead to the following expressions:

$$
\begin{aligned}
&(a)\ \mathrm{US}(j, \mathrm{NY}+2) = \mathrm{US}(j, \mathrm{NY}+1)\mathrm{SLST}\\
&(b)\ \mathrm{UN}(j, \mathrm{NY}+2) = \mathrm{UN}(j, \mathrm{NY}+1)\mathrm{SLNT}\\
&(c)\ \mathrm{VS}(j, \mathrm{NY}+1) = \mathrm{HYCT}[\mathrm{PF}(j, \mathrm{NY}+1) - \mathrm{PEXT}]\\
&(d)\ \mathrm{VN}(j, \mathrm{NY}+1) = \tfrac{1}{2}(1 - \mathrm{STKT})\{(\tfrac{4}{3})\mathrm{VN}(j, \mathrm{NY})\\
&\qquad - (\tfrac{1}{3})\mathrm{VN}(j, \mathrm{NY}-1) - (\tfrac{2}{3})\mathrm{DY}(\Psi_F)/(\Lambda_n + 2\mathrm{M}_n)\\
&\qquad - (\tfrac{1}{3})[(\mathrm{DY}/\mathrm{DX})\Lambda_n(\mathrm{UN}(j, \mathrm{NY}+1)\\
&\qquad + \mathrm{UN}(j, \mathrm{NY}+2) - \mathrm{UN}(j-1, \mathrm{NY}+1)\\
&\qquad - \mathrm{UN}(j-1, \mathrm{NY}+2))]/(\Lambda_n + 2\mathrm{M}_n)\}\\
&(e)\ \mathrm{TN}(j, \mathrm{NY}+2) = \tfrac{1}{2}(1 + \mathrm{STKT})\mathrm{TN}(j, \mathrm{NY}+1)\\
&(f)\ \mathrm{TS}(j, \mathrm{NY}+2) = 1 - \mathrm{TN}(j, \mathrm{NY}+2)\\
&(g)\ \mathrm{PF}(j, \mathrm{NY}+2) = \mathrm{PEXT}, \qquad \text{(A16)}
\end{aligned}
$$

where the index j runs between 2 and NX + 1.

The remaining three walls of the reaction vessel are handled in a completely analogous fashion.

Solving the Finite Difference Equations

Suppose that in some manner we are given the values of the various elements of the "old" network density array, TNO(j, k), pertaining at time, $T = T_o$. If this is the case, the boundary conditions together with the finite difference equations discussed in the preceding sections constitute a large but sparse system of nonlinear simultaneous algebraic equations. In principle, these equations can be solved to give the values of the elements of the network density array, TN(j, k), that pertain at the new time point, $T = T_o + \mathrm{d}T$. The equations also yield the elements of the other six arrays, TS(j, k), PF(j, k), UN(j, k), US(j, k), VS(j, k), and VN(j, k), that pertain after the small time step. Obviously, if we are given a starting point and if we can solve the simultaneous algebraic equations with sufficient accuracy, then by using the network density array derived from the last time step as the starting point for a new time step, we can compute and follow the time evolution of all seven physically important arrays for as long as we wish. The only missing component of this process is an accurate and fast algorithm for solving the simultaneous algebraic equations.

Most algorithms for solving large systems of simultaneous and nonlinear algebraic equations require some sort of quasi-linearization (i.e., one must reduce the nonlinear system to a sequence of linear systems). For the case at hand a good procedure for quasi-linearization is apparent when one observes that the nonlinearities all arise from the coupling between density fields on the one hand and velocity fields and pressure fields on the other. Thus we hold the velocity and pressure fields constant, so that the equations for network mass conservation and excluded volumes constitute a linear subsystem in TN and TS. Similarly, we view the equations for momentum and volume conservation at fixed TS and TN, so that the subsystem is linear in the components of UN, VN, US, VS, and PF.

Having decomposed the system into linear subsystems, we must repeatedly solve the linear subsystems in a cyclical fashion until a fully self-consistent solution emerges. In the case of the density fields, solution of the linear subsystem is easily accomplished by means of a simple point Jacobi iteration. It can be shown that this subiteration must converge very rapidly because the spectral radius of the iteration matrix is $0(\mathrm{d}T)$ as $\mathrm{d}T \to 0$. In our code, a single cycle of point Jacobi corrections for TN and TS is carried out by a subroutine TCRECT. A more sophisticated procedure for computing density corrections is not warranted because this is not the rate-limiting aspect of the overall iteration.

To solve for the pressure and velocity fields, we have examined several iterative procedures (Young, 1971). These procedures yield similar results but differ considerably in their efficiency. For the present discussion, we will restrict ourselves to a brief statement of a very basic iterative technique involving successive calls to three subroutines: VSCRECT, VNCRECT, and PCRECT. This discussison should suffice for those who are simply interested in understanding the biological and physical implications of our computations. Persons who are seriously interested in extending or repeating our calculations should correspond directly with the authors to obtain annotated FORTRAN listings. We will also be happy to discuss various means of accelerating the basic iterative procedure.

Subroutine PCRECT carries out the following operations (modified Richardson's iteration): first, the value of FCV(j, k) is computed for all j and k. If the volume flux into cell (j, k) is negative, then PCRECT reduces the value of PF(j, k). If volume is being gained by cell (j, k), then PF(j, k) is increased. The efficiency of this procedure depends greatly on accurate estimates of the change in PF(j, k) needed to compensate for a given value of the residual of the volume divergence. An array containing such estimates for each cell of the computational grid is generated once per time step by an implicit differentiation procedure.

Subroutine VNCRECT computes pseudoresiduals for the velocity arrays so as to satisfy the two equations of x-momentum conservation at the right edge of cell (j, k) if this edge falls in the interior of the reaction vessel. Pseudoresiduals for VN(j, k) are then computed in a completely analogous fashion. The corrections are applied at interior edges according to an extrapolated Jacobi procedure. Finally, corrections on boundary edges are carried out in accord with the appropriate tangent and normal boundary conditions on the network and solution velocities. These latter corrections are carried out according to a simple Jacobi procedure. Subroutine VSCRECT is similar to VNCRECT except that corrections are computed for the solution velocity array.

Note that the consistent use of the Jacobi procedure in all four subroutines is necessary in order to prevent the occurrence of vorticity related to the ordering. Procedures based on the Gauss-Siedel method were tested and do not work except for one-dimensional problems.

The first task at the start of each time step is to decide if a time step is necessary at all; that is, if $T \geq T_{end}$. Presuming that a time step is necessary, we must then proceed to decide on the size of the time step to be utilized; that is, we must choose a value of $\mathrm{d}T$.

At the start of a computation we have no information about the expected solution, and it is necessary to choose a very conservative time step ($\mathrm{d}T = 10^{-6}$ s is usually safe). For time steps other than the first one, the optimal choice of $\mathrm{d}T$ can be based on information about the existing state of the reaction vessel. If $\mathrm{d}T$ is too small, then effort will be needlessly wasted; if $\mathrm{d}T$ is too large, then the iteration procedure will not converge. The most important constraint on the choice of $\mathrm{d}T$ is the Courant condition

$$\mathrm{d}T < \mathrm{d}T_{\mathrm{Cour}} \equiv \frac{\min[\mathrm{dX}, \mathrm{dY}]}{\max[\mathrm{VNMAX}, \mathrm{VSMAX}]}, \qquad \text{(A17)}$$

where VNMAX and VSMAX are the maximum speeds of the network and solution flow, respectively.

The time step must also be chosen in order to give good resolution of the chemical relaxation processes of network formation and breakdown at all points in the reaction vessel. Since we assume that the chemical reaction is

characterized by a single relaxation time, this condition will be satisfied if

$$dT < T_{eq}. \tag{A18}$$

In order to simultaneously satisfy the constraints of dT, dT_{Cour} is computed, and dT is then chosen according to the formula

$$dT = \min\{\mathrm{DEL}(dT_{Cour}), \mathrm{DEL}(T_{eq}), T_{end} - T\}, \tag{A19}$$

where DEL < 1 is an adjustable numerical parameter.

Having chosen an appropriate value of dT, we next set the value of the TNO array equal to TN from the previous time step. At this point, the actual time step iteration can begin. We repeatedly call VNCRECT, VSCRECT, TCRECT, and PCRECT until a convergence criteria is satisfied. Also, for all but the first time step, we require that at least five cycles of the iteration be carried out, even if the convergence test is satisfied at an earlier stage. On the first time step, we require at least 10,000 cycles before conducting a convergence test.

In conducting the convergence test we must keep track of the size of the adjustments made to the various array elements during the preceding round of corrections. Thus if $|\mathrm{DTN}(j,k)|$ is the L_1 norm of the adjustment to $\mathrm{TN}(j,k)$ made during the preceding call to TCRECT, then we compute a convergence criterion for the network density. TESTTN = $|\mathrm{DTN}(j,k)|/|\mathrm{TN}(j,k)|$, where $|\mathrm{TN}(j,k)|$ is the L_1 norm of $\mathrm{TN}(j,k)$.

In a similar way, we compute convergence criteria for the velocity fields

$$\mathrm{TESTVN} = (|\mathrm{DVN}(j,k)| + |\mathrm{DUN}(j,k)|)/(|\mathrm{VN}(j,k)| + |\mathrm{UN}(j,k)|)$$

$$\mathrm{TESTVS} = (|\mathrm{DVS}(j,k)| + |\mathrm{DUS}(j,k)|)/(|\mathrm{VS}(j,k)| + |\mathrm{US}(j,k)|)$$

and for the pressure field $\mathrm{TESTPF} = |\mathrm{DPF}(j,k)|/|\mathrm{PF}(j,k)|$.

We finally compute a grand convergence criteria TEST = max {TESTTN, TESTVN, TESTVS, TESTPF}, and we allow the iteration to terminate only if TEST ≤ EPS, where EPS is an adjustable numerical parameter. If the convergence test is satisfied, then the time is advanced by an amount dT, and the process begins again.

Choosing the Numerical Parameters

There are four adjustable numerical parameters in our algorithm: DX, DY, DEL, and EPS. DX and DY control the spatial resolution. EPS controls the accuracy of the first few time steps of a computation and is also occasionally important as a check on the accuracy of time steps near critical turning points where vary rapid temporal changes occur. For the bulk of the time steps in a computation, EPS will be irrelevant because temporal continuity implies that the total changes undergone by the seven field variables will approach zero as $dT \to 0$. The propagation of errors through the later time steps can be controlled either by DEL or by adjusting the minimum number of cycles required per time step. The ultimate empirical test of the accuracy of a given computation rests on whether or not changes in DX, DY, EPS, or DEL in a companion computation produce observable changes in significant aspects of the results.

The choice of DX and DY is dictated by the physical need to resolve certain spatial patterns and by considerations of cost. Ideally, the grid spacings should be chosen sufficiently small so that all variations in density, pressure, and velocity are smooth and well-resolved in all portions of the reaction vessel at all times during the computation. Thus the occurrence of structures or patterns defined by only one or two grid cells indicates that increased spatial resolution is required. For a fixed size of reaction vessel, our procedure is to start at a low spatial accuracy and to progressively double the accuracy until there are no further significant effects on the results or until the costs become prohibitive. Usually, if the spatial accuracy is doubled, the costs increase by a factor >4 but <8. If the cost is the limiting factor, then one must either decrease the size of the reaction vessel or one must be satisfied with the subjective process of somehow discriminating between those features of the results that seem sensitive to spatial resolution and those other features that seem to be preserved over a range of resolutions.

For fixed DX and DY, the choice of DEL and EPS is empirically dictated by studying the accuracy after a fixed number of time steps in various trial computations. Starting with initial estimates, DEL and EPS are reduced in stages until no effect of further reduction can be observed. In most cases we find DEL = 0.1 and EPS = 10^{-3} to be adequate.

This work was supported by RCDA K04-AI00966-02 and by grant #R01-AI21002-01 from the National Institutes of Health. Work was also supported by the United States Department of Energy.

Received for publication 23 September 1985 and in final form 22 January 1986.

REFERENCES

Condeelis, J. S., and D. L. Taylor. 1977. The contractile basis of amoeboid movements. V. The control of gelation, solation and contraction in extracts from dictyostelium discoideum. *J. Cell Biol.* 74:901–927.

Hellewell, S., and D. L. Taylor. 1979. The contractile basis of amoeboid movement. VI. The solation-contraction-coupling hypothesis. *J. Cell Biol.* 83:633–648.

Kane, R. E. 1980. Induction of either contractile or structural actin-based gels in sea urchin egg cytoplasmic extract. *J. Cell Biol.* 86:803–809.

Kane, R. E. 1983. Interconversion of structural and contractile actin gels by insertion of myosin during assembly. *J. Cell Biol.* 97:1745–1752.

Pollard, T. D. 1976. The role of actin in the temperature-dependent gelation and contraction of extracts of acanthamoeba. *J. Cell Biol.* 68:579–601.

Stendahl, O. I., and T. P. Stossel. 1980. Actin-binding protein amplifies actomyosin contraction and gelsolin confers calcium control on the direction of contraction. *Biochem. Biophys. Res. Comm.* 92:675–681.

Stossel, T. P., and J. H. Hartwig. 1976. Interactions of actin, myosin, and a new actin-binding protein of rabbit pulmonary macrophages. II. Role in cytoplasmic movement and phagocytosis. *J. Cell Biol.* 68:602–619.

Young, D. M. 1971. Iterative solution of large linear systems. Academic Press, New York.